Geophys. J. Int. (2004) **157,** 1175–1188 doi: 10.1111/j.1365-246X.2004.02254.x

Thermodynamic constraints on seismic inversions

N. M. Shapiro and M. H. Ritzwoller

Center for Imaging the Earth's Interior, Department of Physics, University of Colorado at Boulder, Boulder, CO 80309-0390, *USA.*
E-mails: nshapiro@ciei.colorado.edu (NMS); ritzwoller@ciei.colorado.edu (MHR)

Accepted 2004 January 16. Received 2003 March 26; in original form 2002 May 1

SUMMARY

We discuss two types of physical constraints derived from thermodynamics that can be applied during seismic inversions. The first constraint involves assimilating heat-flow measurements in seismic inversions. This can improve seismic models beneath continents, particularly beneath cratons and continental platforms where uncertainties in crustal radioactive heat production and the anelastic correction are smallest. The second thermodynamic constraint involves replacing ad-hoc seismic parametrizations with physical parameters that describe the thermal state and evolution of the oceanic upper mantle. The inverse problem is, therefore, recast as a hypothesis test to determine if the data are consistent with the thermodynamic model, which here consists of a shallow conductive layer underlain by a convective mantle. We argue that this constraint produces more plausible models of the oceanic lithosphere and asthenosphere and reduces the uncertainty of the seismic model while negligibly degrading the fit to the seismic data in most places.

Key words: heat flow, physical constraints, seismic inversion, thermal models.

1 INTRODUCTION

As with any inverse problem, seismic tomography suffers from limitations dictated by the distribution and quality of seismic data, as well as by trade-offs between diverse structures within the Earth. Phrased differently, it is likely that the Earth possesses a substantial component in the null space of any realistic number and mix of seismic data (e.g. Deal & Nolet 1996). Regularization methods (e.g. Tikhonov, Occam's inversion and so forth) are designed to control the over-interpretation of data by constraining the null-space content of the estimated model, but do not guarantee the physical acceptability of the resulting model nor a model that lies near to the real Earth in model space. These limitations are fundamental. To produce more realistic, physically acceptable earth models requires physical constraints to be applied during seismic tomography.

In this paper, we discuss two types of physical constraints derived from thermodynamics that can be usefully applied during seismic inversions. The first is the assimilation of heat-flow information in the seismic inversion. The second physical constraint imposes theoretical limits on the shape of the temperature curve with depth by explicitly specifying the equations that model the thermal state and evolution of the upper mantle and considering only the solutions to these equations. Relating mantle temperatures to seismic velocities is central to the application of both constraints that we consider. There are uncertainties in this relation as well as the physical parameters needed to combine seismic and heat-flow data. Application of these physical constraints, therefore, requires quantifying uncertainties and tracking them in the inversion along with the intrinsic uncertainties in the seismic parameters.

To facilitate the error propagation, we perform a Monte-Carlo inversion. The seismic data are surface wave dispersion maps of broad-band group and phase speeds. The group velocity measurements were made at the University of Colorado at Boulder (e.g. Ritzwoller & Levshin 1998; Ritzwoller *et al.* 2001) and the phase velocity data were donated by Harvard University and Utrecht University (Trampert & Woodhouse 1995; Ekström *et al.* 1997; Ekström & Dziewonski 1998). The inversion is divided into two steps. The first step is surface wave tomography (e.g. Barmin *et al.* 2001; Ritzwoller *et al.* 2002) in which the measured dispersion curves are inverted to produce 2-D maps of the geographical distribution of phase and group speeds for individual periods and wave types. The dispersion maps are found with diffraction tomography, which is based on a physical model of the surface wave Fresnel zone that accounts for path-length dependent sensitivity, wavefront healing and associated diffraction effects. As a result, we estimate at each geographical location four dispersion curves: the phase speed of Rayleigh and Love waves at periods between 40 and 150 s, and group speeds between 16 and 200 s. In the second step, on a $2^\circ \times 2^\circ$ grid worldwide, these four dispersion curves are inverted to obtain a local radially anisotropic shear velocity model using a Monte-Carlo method (Shapiro & Ritzwoller 2002), as illustrated in Fig. 1. We randomly generate a large number of models and select only those that fit the observed dispersion curves acceptably. This method is fully non-linear and results in an ensemble of models from which we estimate model uncertainty.

The application of the thermal constraints in the seismic inversion involves a straightforward modification of the Monte-Carlo sampling, as illustrated in Fig. 2. Heat-flow observations and theoretical

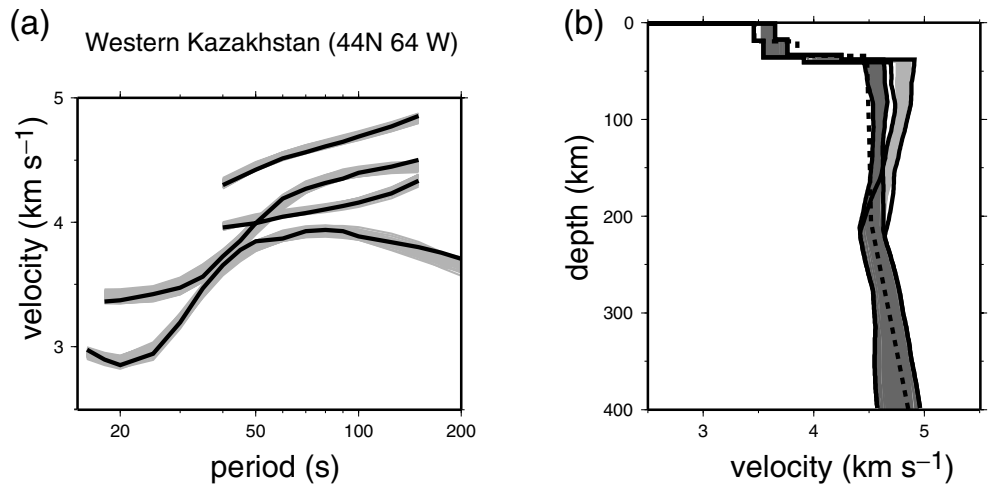

Figure 1. Results of the inversion for an ensemble of acceptable shear velocity models at a location in western Kazakhstan (44°N, 64°E) using an ad-hoc seismic parametrization. (a) Four dispersion curves obtained from surface wave velocity maps (thick black lines) and the predictions from the ensemble of acceptable models (gray lines). (b) The ensemble of acceptable radially anisotropic models, where v_{sv} and v_{sh} are shown with dark and light gray shades, respectively. The corridor of acceptable values is indicated with the solid black lines and the 1-D model ak135 (Kennett *et al.* 1995) is plotted as the dashed line for reference.

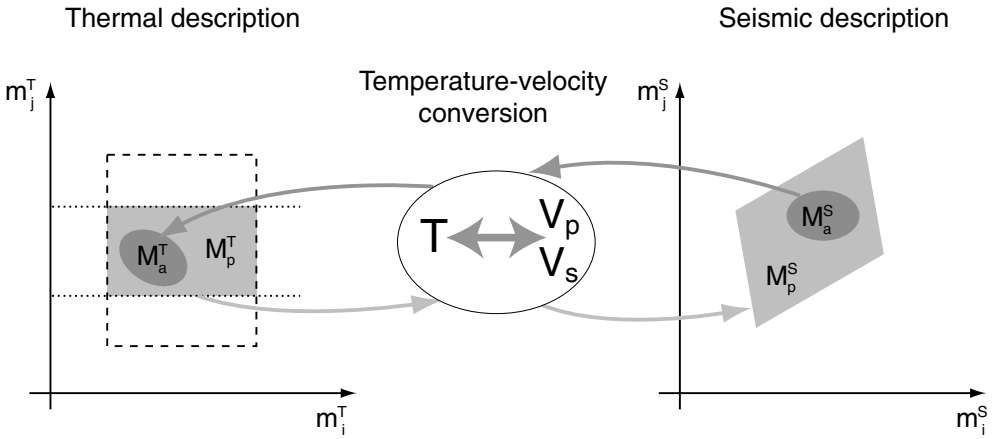

Figure 2. Schematic representation of the Monte-Carlo seismic inversion based on a thermal description of the model. The thermal description (left panel) is constrained by the heat-flow data (horizontal dotted lines) and theoretical constraints on the thermal structure and evolution of the mantle (dashed rectangle). These constraints delimit the range of physically plausible thermal models M_p^T (light shaded area on the left panel). Using a velocity–temperature, this range is converted into a range of physically plausible seismic models M_p^S (light shaded area on the right panel). Random sampling within M_p^S identifies the ensemble of acceptable seismic models M_a^S (dark shaded area on the right panel). Finally, this ensemble is converted into the ensemble of acceptable thermal models M_a^T (dark shaded area on the left panel).

constraints on temperature are used to delimit the range of physically plausible temperature models, which is then converted into the range of physically plausible seismic models. The Monte-Carlo method randomly samples the models within this range and identifies the subset of seismic models that acceptably satisfy the seismic data. By reconverting the seismic velocities back into temperature, the ensemble of acceptable temperature models is identified.

Heat-flow measurements are most numerous on continents, so we will discuss the assimilation of these data in seismic inversions only at continental locations. The theoretical constraints on the mantle temperature profile involve explicitly estimating parameters in the solution of the equations that model the thermal state of the upper mantle. The thermal evolution of the oceanic mantle is probably best understood and we will explicate this method only for the oceanic lithosphere.

The method we propose ultimately emerges as a hypothesis test to determine whether the seismic data are consistent with the thermal constraints. If they are consistent, we show that in some cases the range of acceptable seismic models can be substantially reduced, producing smaller uncertainties and presumably a better model. In addition, the model that we estimate is fundamentally a temperature model, which may be closer to what is desired in many cases than the intrinsic seismic speeds. There have been numerous previous studies that have explored the relationship between seismic wave speeds, temperature and composition (e.g. Yan *et al.* 1989; Furlong *et al.* 1995; Goes *et al.* 2000; Röhm *et al.* 2000; Trampert *et al.* 2001; van Wijk *et al.* 2001). Recent work has concentrated on estimating variations in temperature and perhaps composition at the length-scales of seismic tomography. Our approach is the converse of most of these earlier studies. We aim to improve the tomography

by applying information about temperature and heat flow to ensure the physical reasonableness of the seismic model.

In Section 2, we describe the relation between the seismic velocities and temperatures in the upper mantle and attempt to characterize the uncertainties in this conversion. The heat-flow constraint, with examples in several continental regions, is discussed in Section 3. In Section 4, we investigate the application of thermodynamic constraints on the suboceanic upper mantle.

2 CONVERSION BETWEEN SEISMIC VELOCITIES AND TEMPERATURE IN THE UPPER MANTLE

Converting between seismic velocities and thermodynamic parameters, such as temperature and pressure, has been the subject of numerous studies (e.g. Duffy & Anderson 1989; Sobolev *et al.* 1996; Goes *et al.* 2000). Here, we use the method of Goes *et al.* (2000) where the isotropic seismic velocities are converted to temperatures and vice versa based on laboratory measured thermoelastic properties of mantle minerals and models of the average mineralogical composition of the mantle beneath different tectonic provinces. We summarize the salient aspects of this procedure in Appendix A. The key issue is to track uncertainties in the conversion, which we discuss further here.

2.1 Uncertainties associated with velocity–temperature conversion

Uncertainties in the seismic velocity–temperature relationship result from a number of sources, including uncertainties in mantle composition, in the thermoelastic properties of individual minerals, and the anelastic correction. The properties of the principal mantle minerals are measured in laboratories with quite high precision and, therefore, uncertainties in these parameters are not major contributors to errors in the velocity–temperature conversion. The most important uncertainties relate to mantle mineralogical composition and the anelastic correction.

2.1.1 Uncertainties in mantle composition

Variations in mantle composition between different tectonic and geological provinces are roughly constrained by studies of mantle xenoliths (e.g. McDonough & Rudnick 1998). A prominent compositional heterogeneity within continents is the difference between the depleted on-cratonic mantle and the off-cratonic mantle (Table 1). Seismic velocities computed at 60 km depth by using these two different compositions are shown in Fig. 3. Compositional uncertainties have strongest effect at low temperatures and affect *P*-wave velocity more than *S*-wave velocity in an absolute sense. The velocities computed with these two compositions differ by no more than approximately 2 per cent. Compositional variations within a single tectonic regime are expected to be smaller and

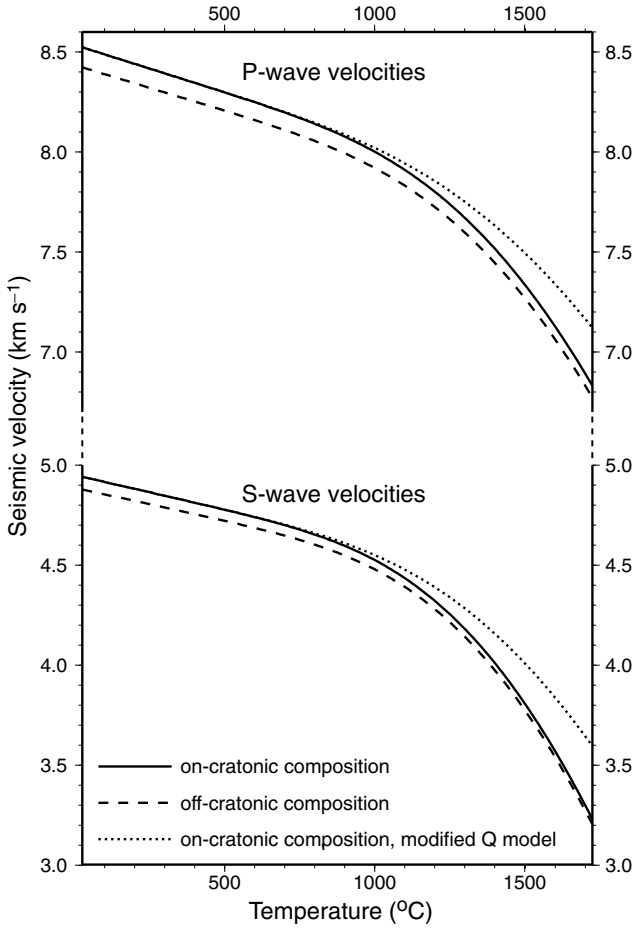

Figure 3. *P*- and *S*-wave velocities calculated at 60 km depth using eqs (A1)–(A13). Solid lines show the results for on-cratonic composition with the normal anelastic correction ($A = 0.049$). Dashed lines show the results for the off-cratonic composition with the normal anelastic correction. Dotted lines are the results for the on-cratonic composition with a reduced anelastic correction ($A = 0.074$).

we estimate the uncertainty in the velocity–temperature conversion caused by composition to be approximately 1 per cent, which we believe is conservative.

2.1.2 Uncertainties in the anelastic correction

The anelastic properties of mantle materials are not as well constrained by laboratory measurements as the elastic properties. Therefore, the anelastic correction is a large source of uncertainty in the velocity–temperature conversion. To quantify the effect of the errors in the anelastic parameters, we calculated seismic velocities for two different values of A in eq. (A11). The results for $A = 0.049$ and $A = 0.074$ are shown in Fig. 3 with solid and dotted lines, respectively. At 1500 °C, changing A by 50 per cent results in almost a

Table 1. Mineralogical composition used for the upper mantle (e.g. Dick *et al.* 1984; McDonough & Rudnick 1998).

	Olivine (per cent)	Orthopyroxene (per cent)	Clinopyroxene (per cent)	Garnet (per cent)	Spinel (per cent)	X_{Fe}
On-cratonic	83	15	0	2	0	0.086
Off-cratonic	68	18	11	3	0	0.1
Oceanic	75	21	3.5	0	0.5	0.1

10 per cent variation of the shear velocity. This means that the uncertainties resulting from the anelastic correction are large at high temperatures, but negligible at temperatures below approximately 1100 °C.

2.1.3 Other, unmodelled uncertainties

The presence of substantial quantities of melt and/or water in the mantle would affect seismic velocities strongly (e.g. Karato & Jung 1998). Unfortunately, a rigorous quantitative description of these effects does not exist yet. The influence of water and melt probably can be neglected in old continental lithosphere, which is believed to be dry as a result of episodes of melting in the formation of cratons and too cold for the presence of melt in the uppermost mantle. Because the uncertainty in the anelasticity correction is also small for cold materials, we expect that the velocity–temperature relation works better in old continental areas, while the uncertainties in this relation are largest in regions that have undergone recent lithospheric rejuvenation.

3 APPLICATION OF THE HEAT-FLOW CONSTRAINT BENEATH CONTINENTS

Surface heat flow is correlated with surface tectonics, both within continents and oceans. In oceans, average heat flow decreases with increasing seafloor age as a result of the cooling of the oceanic lithosphere (e.g. Stein & Stein 1992). A similar pattern is observed in continents where heat flow is lowest for the Archaean cratons (e.g. Nyblade & Pollack 1993; Rudnick *et al.* 1998). This global correlation suggests a relation between the surface heat flow and the thermal regime of the upper mantle. This relation is less straightforward in continents where it is masked by the distribution of the radioactive heat production in the continental crust (e.g. Nyblade & Pollack 1993).

Various researchers have used heat-flow observations to infer the temperature structure of the continental lithosphere (e.g. Artemieva & Mooney 2001). These inversions are classically ill-posed, as they formally attempt to estimate the temperature profile from a single measurement, the heat flow at the surface. They, therefore, require *a priori* information on the distribution of the radioactive heat production as well as simplifications to the thermal equation. In addition, there are large uncertainties in the heat-flow measurements. For these reasons, uncertainties tend to be rather large in temperature profiles estimated from thermodynamic observables alone, as discussed in detail by Artemieva & Mooney (2001), and grow quickly as the mantle is penetrated beneath the Moho. Geotherms predicted from seismic models also have large uncertainties, as we discuss further below. Seismic geotherms have been compared with those predicted from heat-flow observations with mixed results (e.g. Röhm *et al.* 2000; Goes *et al.* 2000) and have been limited by the lack of uncertainty estimates on either the seismic or thermal models.

Fortunately, constraints on the thermal structure of the mantle derived from heat-flow and seismic data are complementary. Here, we propose to combine both types of measurements in a single inversion in order to improve both the seismic and temperature models. As seismologists, we see this as assimilating heat-flow measurements into the seismic inversion, but one could equally well see this as assimilating seismic data into the heat-flow inversion. Therefore, estimating uncertainties in both the seismic and heat-flow inversions is crucial to combine heat-flow and seismic data.

The estimation of uncertainties in the seismic surface wave inversion is performed with a Monte-Carlo method, as described by Shapiro & Ritzwoller (2002). Here, our discussion will concentrate on estimating the uncertainties in the heat-flow inversion. Because of the nature of the thermal equation, this uncertainty grows with depth, so we limit the objective of the heat-flow inversion to constrain just one parameter in the temperature model: namely, the temperature (or seismic velocity) at the top of the mantle. Deeper structures are estimated from the seismic data alone.

Table 2. Thermal parameters of the crust and upper mantle (e.g. Rudnick *et al.* 1998; Artemieva & Mooney 2001).

	Q (μW m^{-3})	k (W m^{-1} K^{-1})	κ (m^2 s^{-1})
Cratonic crust	0.3–0.7	2.5–3.0	1×10^{-6}
Off-cratonic crust	0.4–1.4	2.5–3.0	1×10^{-6}
Upper mantle	0.0	4.0	1×10^{-6}

3.1 Constraining temperature at the top of the mantle with heat-flow data

We assume that the thermal structure of the crust can be approximated by the steady-state solution of the 1-D thermal conductivity eq. (B5) with boundary conditions eqs (B4) and (B6). If the surface heat flow q_0, the distribution of crustal heat production $H(z)$, and thermal conductivity $k(z)$ are known, eq. (B5) can be solved for the geotherm $T(z)$. These parameters, however, are known only approximatively, so the estimated temperature is uncertain. To estimate this uncertainty, we consider surface heat flow to lie in the interval $[q_0 - dq_0, q_0 + dq_0]$ and also consider a range of values for the average heat production and thermal conductivity in the crust: $[k_{\min}, k_{\max}]$ and $[H_{\min}, H_{\max}]$. Following the properties of the steady-state solutions described in Appendix A2, we use $q_0 + dq_0$, $k_{\min}$, and $H_{\min}$ to compute the higher (warmer) geotherm, and $q_0 - dq_0$, $k_{\max}$, and $H_{\max}$ to compute the lower (cooler) geotherm. The ranges of allowed values for crustal conductivity and radioactive heat production are taken from Rudnick *et al.* (1998) and are shown in Table 2.

Fig. 4 presents an example of geothermal bounds calculated at two locations, one is a stable craton (Canadian shield, 50°N, 76°W) and the other is a tectonically active region (SE Utah, 38°N, 110°W). We take heat-flow measurements by applying a Gaussian spatial smoothing function ($\sigma = 200$ km) to the heat-flow database of Pollack *et al.* (1993). As uncertainties in the heat-flow measurements we use differences in average heat flow reported for similar tectonic provinces around the world. Rudnick *et al.* (1998) report that $dq_0 \approx 10$ mW m^{-2} for cratonic regions and $dq_0 \approx 17$ mW m^{-2} for non-cratonic regions. Regional uncertainties will be smaller than these values and we use uncertainties of $dq_0 \approx 5$ mW m^{-2} and $dq_0 \approx 10$ mW m^{-2} for cratonic and non-cratonic regions, respectively. The heat-flow measurements used in this paper are summarized in Table 3.

Fig. 4 shows that the uncertainty in the temperature estimated from surface heat-flow increases with depth, which is the reason we use heat-flow data only to constrain the temperature at the top

Table 3. Heat-flow values, taken from Pollack *et al.* (1993), at the four locations considered.

Location	Lat.	Long.	q_0 (mW m^{-2})	dq_0 (mW m^{-2})
Canadian shield	50°N	76°W	35	5
Russian platform	64°N	40°E	37.5	5
Southern Germany	50°N	10°E	70	10
Southeastern Utah	38°N	110°W	80	10

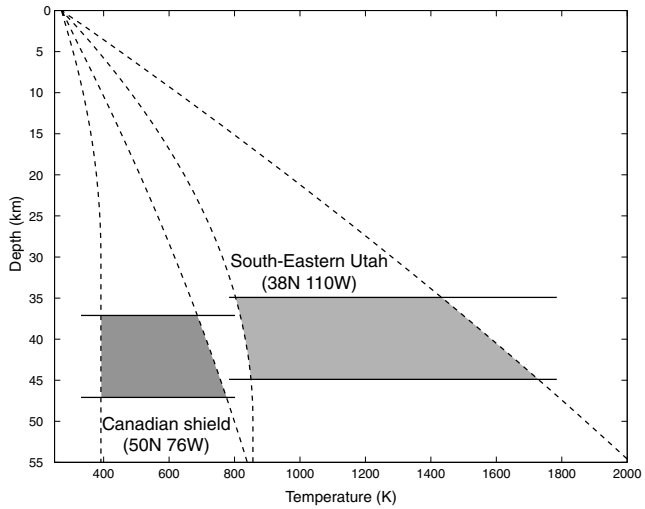

Figure 4. Heat-flow constraints on the temperature at the top of the mantle calculated with eq. (B5) and boundary conditions eqs (B4) and (B6) at two locations: (i) the Canadian shield (50°N, 76°W) and (ii) southeastern Utah (38°N, 110°W). The values of the heat-flow and crustal thermal parameters are presented in Tables 2 and 3. Dashed lines show extreme geotherms. Horizontal solid lines show the allowed range of Moho depths (CRUST2.0 ±5 km). Shaded areas define the regions of allowed temperatures at the top of the mantle.

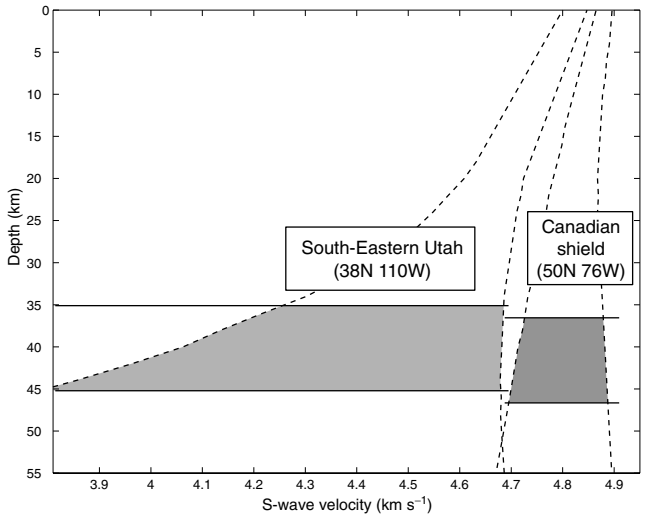

Figure 5. Similar to Fig. 4, but for the heat-flow constraints on the shear velocity at the top of the mantle. Extreme geotherms have been converted into velocity limits (dashed lines) by inverting eqs (A1)–(A13).

of the mantle: i.e. just below the Moho boundary. The location of this boundary is also known with some uncertainty. We use the global model CRUST2.0 (Laske, private communication), which is a refinement of CRUST5.1 (Mooney *et al.* 1998), as the *a priori* model of crustal thickness. We allow a perturbation of the Moho depth of ± 5 km. Extreme geotherms combined with the range of allowed Moho depths define an area of allowed temperatures at the top of the mantle as shown in Fig. 4.

The uncertainty in the estimated temperature is smaller beneath cratons than beneath tectonically active regions because (i) there are smaller uncertainties in the thermal parameters in cratonic than in non-cratonic regions and (ii) the lower temperatures in cratonic regions are less sensitive to uncertainties in the anelastic behaviour of mantle materials (Fig. 3). The heat-flow constraint will tend to be most useful in stable continental areas. There is a caveat to this, however. An upper bound on temperatures in tectonically active regions could be applied at the melting temperature of the lower crust and uppermost mantle. This would reduce the uncertainties in the inferred temperatures considerably. With the application of the upper bound on temperatures, heat-flow measurements would become a more powerful constraint in tectonically active regions.

3.2 Constraining the shear velocity at the top of the mantle

Using the velocity–temperature relation described by eqs (A1)–(A13) and illustrated in Fig. 3, the areas of allowed temperatures can be converted to areas of allowed shear velocities at the top of the mantle. The results for two locations are shown in Fig. 5. As with temperatures, heat-flow data produce stricter bounds on the shear velocities in cratonic areas than in active tectonic areas. The uncertainties in seismic velocity in the tectonically active region would be reduced by applying an upper bound on allowed temperatures, as discussed in the previous section. However, the higher mantle temperatures in the tectonically active region mean that the anelastic correction is larger. In the tectonically active region, uncertainties in the anelastic correction dominate the uncertainties in the seismic velocities inferred from temperatures that result from the heat-flow inversion.

3.3 Surface wave inversion constrained by heat-flow data

We apply the heat-flow constraint during the Monte-Carlo inversion of surface wave dispersion using the area of allowed shear velocities at the top of the mantle. Only the models with sub-Moho velocities lying within the allowed area are considered to be acceptable.

To test the usefulness of the heat-flow constraint, we consider four locations (Table 3): two in cratonic regions (Canadian shield, Russian platform) and two in regions that have undergone recent tectonic deformation (southern Germany, southeastern Utah). Results of the surface wave inversion in the Canadian shield with and without the heat-flow constraint are shown in Fig. 6. The heat-flow constraint significantly reduces the range of acceptable seismic models. A similar result is obtained for the Russian platform (Fig. 7). In tectonically active regions, however, the heat-flow constraint is not as useful. In southern Germany (Fig. 8), the constraint somewhat reduces the uncertainty of the seismic model while in southeastern Utah (Fig. 9), it has no appreciable effect. In southeastern Utah, the temperature bounds that emerge from the heat-flow constraint are broader than the ensemble of seismic models defined by the seismic data alone.

In conclusion, heat-flow data are most useful to improve seismic models in cratons or continental platforms. In active tectonic regions, the constraints on seismic velocity in the uppermost mantle placed by heat-flow data are weaker, particularly as a result of larger uncertainties in the interconversion between temperature and seismic velocity. Heat flow could also be applied as a constraint in oceanic areas. Because of the simple structure and relative thinness of the oceanic crust, the uncertainty of the heat-flow constraint in oceans is expected to be smaller than in continental areas. This awaits further exploration as databases of oceanic heat-flow measurements develop.

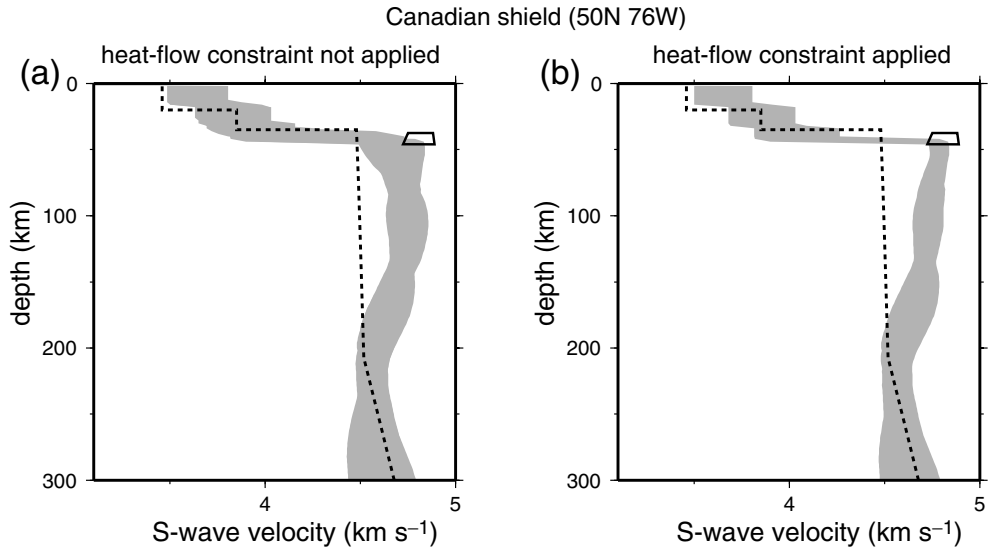

Figure 6. Results of the surface wave inversion at a location in the Canadian shield (50°N, 76°W). The shaded zones identify the ensemble of acceptable models for isotropic shear velocity [$v_s = (v_{sh} + v_{sv})/2$]. The dashed lines are the 1-D model ak135 (Kennett *et al.* 1995), for reference. Black polygons mark the area of allowed shear velocities at the top of the mantle estimated from the heat-flow data. (a) Results without the heat-flow constraint. The black polygon is included for reference only. (b) Results with the heat-flow constraint. All models pass through the black polygon.

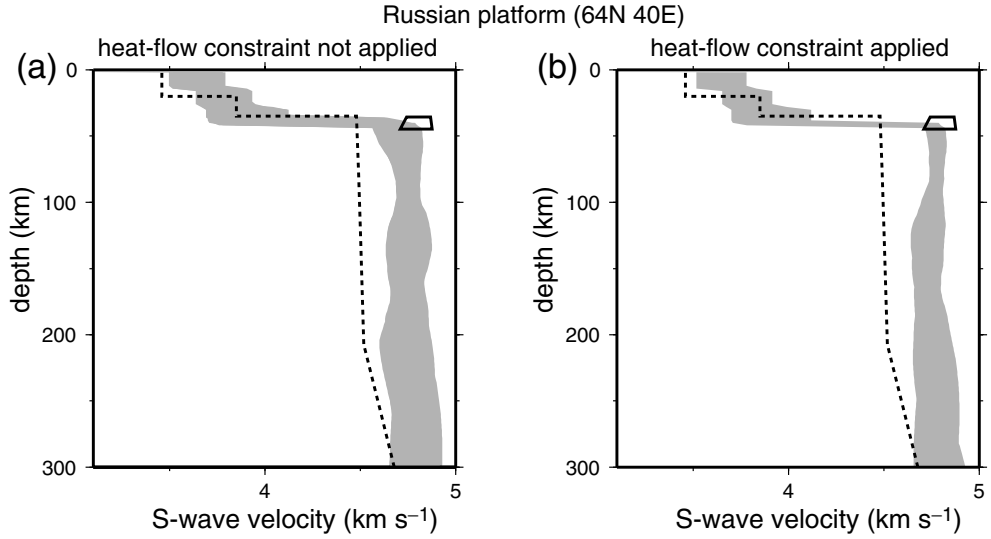

Figure 7. Similar to Fig. 6, but for a second cratonic region, the Russian platform (64°N, 40°E).

4 THERMAL STRUCTURE OF THE OCEANIC LITHOSPHERE

As we show, seismic models of the oceanic lithosphere would benefit from added constraints to ensure physical plausibility. The physical constraints we will apply are based on the simple physical model of heat transfer in the oceanic upper mantle shown in Fig. 10 in which a conductive layer is underlain by a convective mantle. This thermodynamical model is effected by a thermal parametrization that represents conductive and convective cooling in each layer smoothly joined by a transition region.

4.1 Ad-hoc seismic parametrization of the oceanic upper mantle

Figs 11(a)–(c) show the results of the surface wave inversion at a location in the southern Pacific (44°S, 134°W) where lithospheric age is *ca* 48 Myr (Mueller *et al.* 1997). Figs 11(d)–(f) show similar results for a location in the northern Pacific (32°N, 160°W) where lithospheric age is *ca*101 Myr. Several physically questionable features are apparent in the inferred temperature profiles, particularly in Fig. 11(f), such as the constant average temperature between depths of 20 and 40 km and the temperature decrease below 200 km. These problems are partially caused by the ad-hoc nature of the seismic basis functions, which are not designed specifically to model temperature anomalies in the oceanic upper mantle. The cubic B-spline parametrization used by Shapiro & Ritzwoller (2002) apparently over-parametrizes the oceanic upper mantle, resulting in non-physical vertical oscillations that are only apparent when one inspects the temperatures inferred from the seismic model. Fig. 12 shows the difference between several randomly selected members of the ensemble of acceptable models beneath the northern Pacific location, displaying these vertical oscillations. Differences between

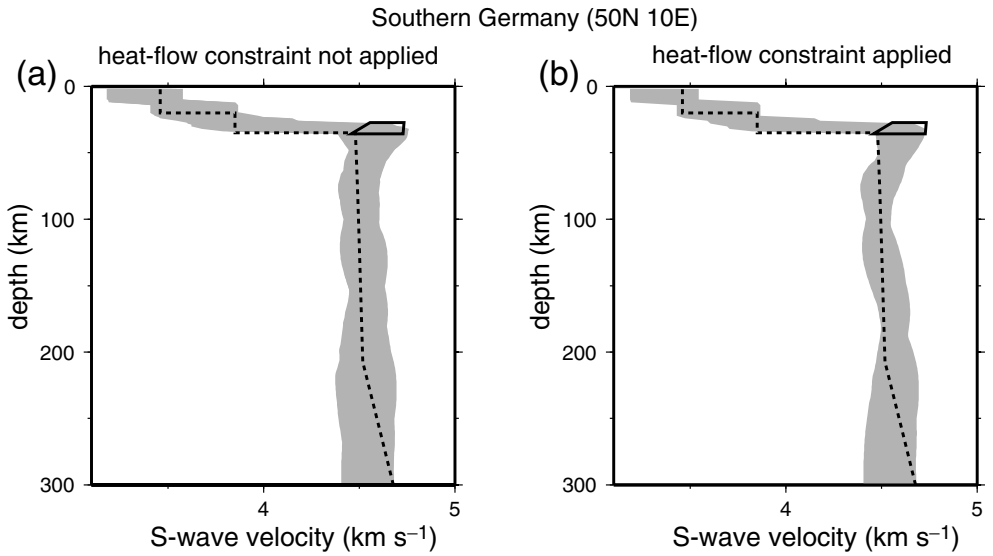

Figure 8. Similar to Fig. 6, but for a region that has undergone recent tectonic deformation, a location in southern Germany (50°N, 10°E).

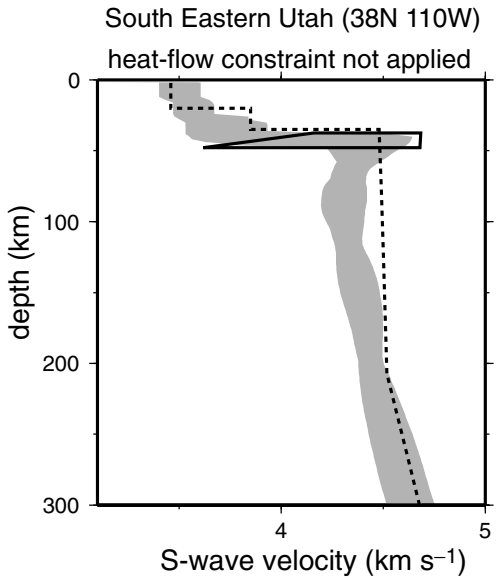

Figure 9. Similar to Fig. 6, but for a second region that has undergone recent tectonic deformation, a location in southeastern Utah (38°N, 110°W). The heat-flow constraint does not change the ensemble of acceptable models from those that result from seismic data alone, so only a single panel is shown.

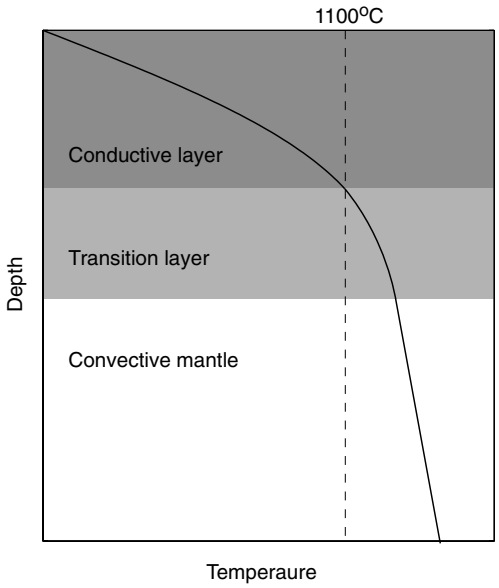

Figure 10. Model of the suboceanic upper mantle used to define the thermal parametrization. The solid line represents an allowed temperature profile.

the acceptable models are unconstrained by the Monte-Carlo inversion and are, therefore, effectively in the null space of the seismic data.

Another problem in oceanic regions for the seismic parametrization used by Shapiro & Ritzwoller (2002) is a fixed *P*-to-*S* velocity ratio. This has no significant effect on relatively deep structures because surface waves are not sensitive to *P*-wave velocities at large depths. However, the Rayleigh waves have non-negligible sensitivity to v_p down to approximately one eight of a wavelength (e.g. Dahlen & Tromp 1998); i.e. to the *P*-wave speed in the crust and the upper part of the oceanic lithosphere at long periods. As a consequence, unrealistic *P*-to-*S* velocity scaling can affect the result of the inversion at depths shallower than 50 km. Finally, it is also necessary to apply stronger constraints on crustal structure than applied by Shapiro & Ritzwoller (2002), which was oriented more toward continental areas where strong variations in the crustal structure are more likely.

These considerations together motivate the application of physical constraints on the seismic model beneath oceans. Presumably similar problems exist beneath continents as well.

4.2 Thermal parametrization of the oceanic upper mantle

To overcome the artefacts of ad-hoc seismic parametrizations, we explicitly apply thermodynamic constraints on the allowed shear velocities by developing a physically motivated parametrization. The idea is to parametrize the thermal structure of the upper mantle in terms of the thermal model shown in Fig. 10 and then to convert the thermal model into *P*- and *S*-wave velocities using eqs (A1)–(A13).

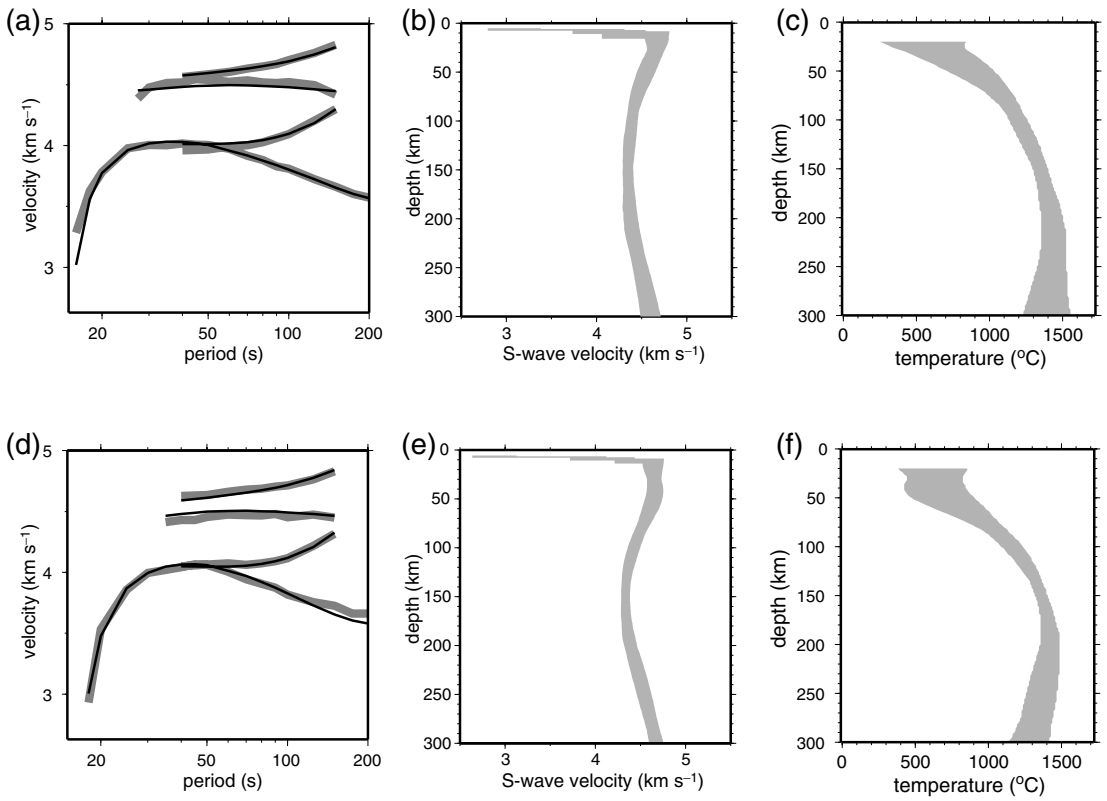

Figure 11. The seismic model and inferred temperature at two locations in the Pacific using the ad-hoc seismic parametrization of Shapiro & Ritzwoller (2002). (a)–(c) Results of the surface wave inversion for a location in the southern Pacific ocean (44°S, 134°W). (a) Dispersion curves, similar to Fig. 1(a). (b) The shaded area defines the ensemble of acceptable models [isotropic part, $v_s = (v_{sv} + v_{sh})/2$]. (c) The shaded area defines the allowed temperatures predicted from the ensemble of acceptable seismic models. (d)–(f) Similar to (a)–(c), but for a location in the northern Pacific (32°N, 160°W).

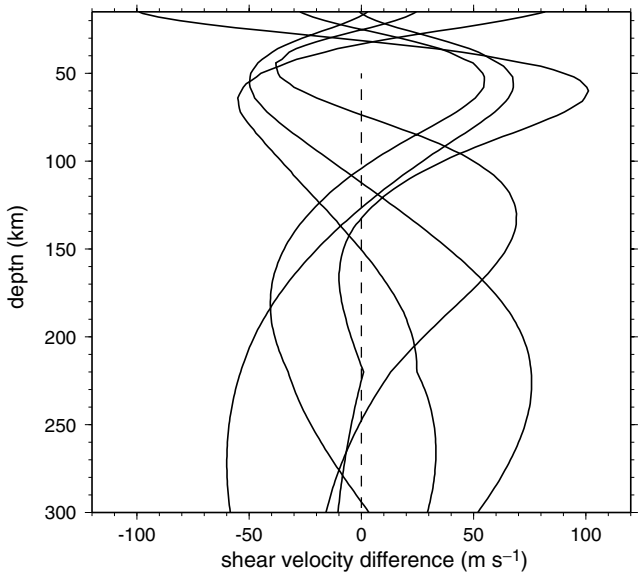

Figure 12. Differences in shear velocities between five randomly selected pairs of acceptable models at the northern Pacific location (32°N, 160°W). These profiles are in the effective null space of the data.

We assume that heat transfer in the shallow part of the upper mantle is controlled by conduction. This conductive layer is separated from the convective mantle by a transition layer. The temperature profile within the conductive layer is described by the half-space cooling solution given by eq. (B7). Following Appendix B, we fix the mantle temperature $T_m = 1300$ °C and describe the conductive part of the model with one parameter: i.e. cooling age τ_c. We consider the conductive and convective layers to be thermally decoupled, which implies that the parameters describing these two layers are independent. In the convective layer, we fix the adiabatic thermal gradient D_a to 0.5 °C km^{-1} (Turcotte & Schubert 1982), which leaves potential temperature T_p (Appendix B) as the single free parameter. The transition layer provides a smooth transition between the conductive and convective parts of the model. The thicknesses of the conductive and the transition layer depend on the cooling age. We define the bottom of the conductive layer as the depth at which the temperature calculated with eq. (B7) is equal to 1100 °C. The thickness of the transition layer is set to 70 per cent of the thickness of the conductive layer.

The mantle temperature profile, therefore, is described by only two unknowns: the cooling age τ_c and the potential temperature in the convective mantle T_p. These two parameters replace the four cubic B-splines used by Shapiro & Ritzwoller (2002). Fig. 13 shows the temperature and the shear velocity quality factor predicted by such a simple thermal model with $T_p = 1300$ °C for four different cooling ages. The temperature decreases and the quality factor increases with increasing cooling age. The value of the quality factor predicted for the asthenosphere beneath the young ocean is roughly consistent with existing observations (e.g. Canas & Mitchell 1981; Chan *et al.* 1989).

Results of the inversion using the thermal model are shown in Fig. 14 for the same two locations in the Pacific shown in Fig. 11. Comparing the inversions using the thermal and seismic

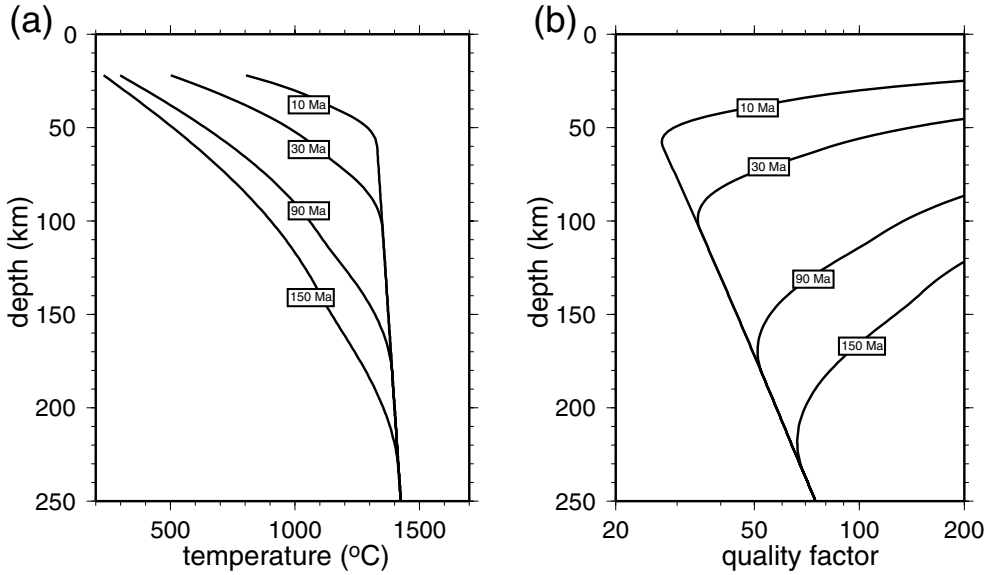

Figure 13. Thermal models of the suboceanic upper mantle with a potential temperature $T_p = 1300$ °C and four different cooling ages: 10 Myr, 30 Myr, 90 Myr and 150 Myr. (a) Temperature as a function of depth. (b) Shear quality factor as a function of depth.

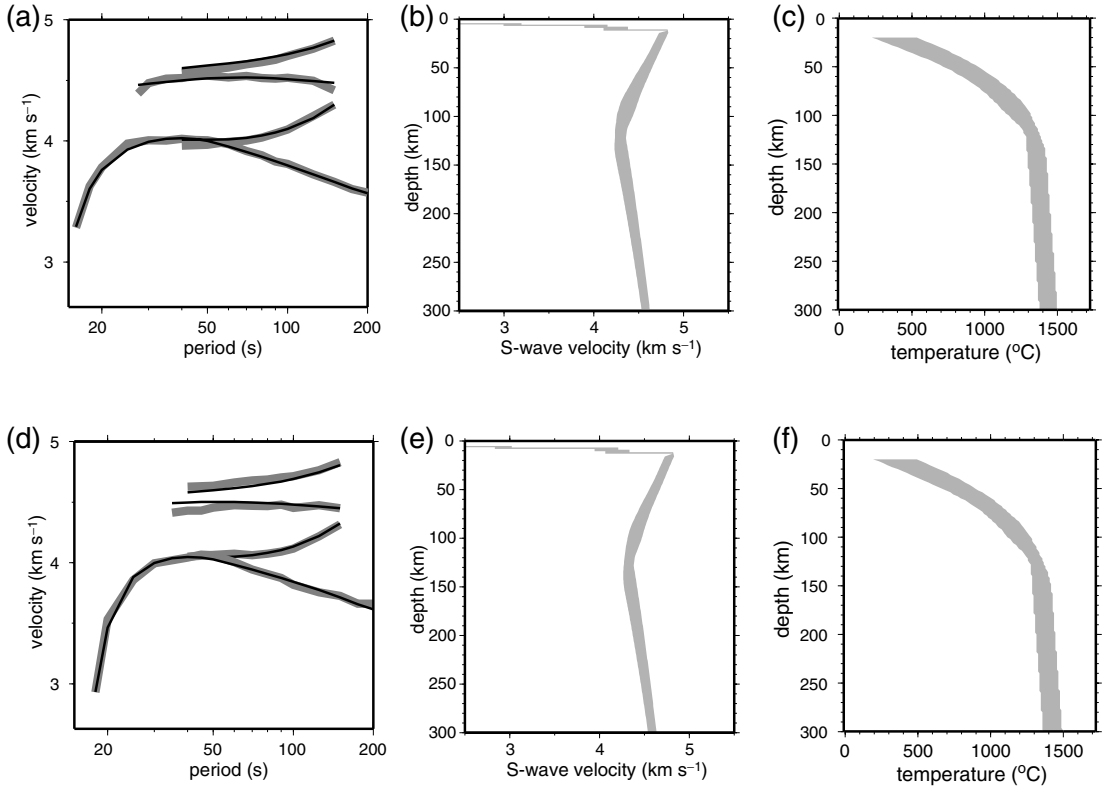

Figure 14. Results of the surface wave inversion with the thermal parametrization at two locations in the Pacific ocean (44°S, 134°W and 32°N, 160°W), similar to Fig. 11.

parametrizations reveals that, while there is little difference in the misfit to the observed dispersion curves, the inversion with the thermal parametrization has several distinct advantages. First, the non-physical artefacts disappear from the temperature profiles. Temperature increases monotonically with depth. Secondly, the uncertainties in seismic velocities and temperatures are significantly reduced. Thirdly, the parameters used in the thermal parametrization are more convenient for interpretation than the spline coefficients used in the ad-hoc seismic parametrization. For example, consider the estimated range of cooling ages. At the location in the southern Pacific (44°S, 134°W), τ_c ranges between 33 and 63 Myr and the lithospheric age (48 Myr) lies within these bounds. However, at the northern Pacific location (32°N, 160°W), the estimated cooling age is systematically lower than the age of the lithosphere (40–72 Myr

compared with 101 Myr). This result agrees with the topographic flattening and increased heat flow of old lithosphere compared to expectations from lithospheric age alone (e.g. Parsons & Slater 1977; Stein & Stein 1992). An advantage of using the thermal parametrization is that an estimated cooling age with uncertainties results directly from the Monte-Carlo inversion.

5 DISCUSSION

We discussed the application of two types of thermodynamic constraints applied in the inversion of seismic surface wave data. First, we considered how heat-flow measurements can be used to improve seismic models beneath continents. Our results show that the uncertainties in the heat-flow measurements and the crustal radioactive heat production are small enough in cratonic areas to ensure that the heat-flow constraint is useful. In tectonically active areas, however, the uncertainties in temperature estimated from the heat-flow data may be too large to improve the seismic models. However, further constraints on allowed temperatures are possible that would reduce the range of acceptable temperatures models. It is likely that the heat-flow constraint also will be useful in oceanic areas wherever reliable heat-flow measurements exist.

The second thermodynamic constraint involves explicitly solving for variables in a thermodynamic model of the thermal state and evolution of the upper mantle. The main idea is to parametrize the temperature profile in terms of these variables, such as thermal age and potential temperature, and then to convert to seismic velocities. We develop this thermal parametrization for the oceanic upper mantle consisting of a shallow conductive layer underlain by a convective mantle with an adiabatic temperature gradient. The temperature profile within the conductive layer is taken from a cooling half-space. The inversion with the thermal parametrization produces more plausible models and reduces the uncertainty of the seismic model, while the fit to the observations remains approximately the same as the inversion with a purely ad-hoc seismic parametrization. As Fig. 15 illustrates, similar thermal parametrizations may be warranted for the continental lithosphere.

We believe that these constraints, when applied systematically, will improve upper-mantle seismic models, at least beneath cratons and continental platforms and for the oceanic lithosphere. The heat-flow constraint has been successfully applied to improve the mantle model over the large part of the Canadian shield (Shapiro *et al.* 2004) where the high-quality heat-flow data are available. Further efforts in the development of a heat-flow database (including crustal radioactive heat production and thermal conductivity) are justified, therefore, at least in non-tectonic areas, and may be needed prior to the systematic application of the heat-flow constraint. Systematic application of the theoretical constraint on the shape of the temperature profile in the oceanic mantle is more straightforward, however, and we recently applied it to improve upper mantle models in the Pacific (Ritzwoller *et al.* 2004) and in the southeast Indian ocean (Ritzwoller *et al.* 2003). An example is presented in Fig. 16, which shows that some of the substantial variability in the oceanic lithosphere that appears with an ad-hoc seismic parametrization may be questionable on physical grounds and is not needed to fit the seismic data. Similar thermal modelling can be performed in subduction zones, as the subducting lithosphere heats up as it penetrates into the mantle. At least in motivation, this application would be similar to previous work by Spencer & Gubbins (1980), Deal *et al.* (1999) and Deal & Nolet (1999).

ACKNOWLEDGMENTS

The application of heat flow as a constraint in the seismic inversion was inspired by conversations with Walter Mooney. The authors are grateful to Shijie Zhong, Claude Jaupart and Jean-Claude Mareschal for numerous discussions and to Irina Artemieva for providing us with the results of her heat-flow inversions at an early stage of research. Irina Artemieva and Andrew Nyblade provided critical and very constructive reviews. The authors are also particularly grateful to Jeannot Trampert at Utrecht University and Michael Antolik, Adam Dziewonski and Goran Ekström at Harvard University for providing phase velocity measurements. Gabi Laske provided CRUST2.0 prior to publication. All maps were generated with the

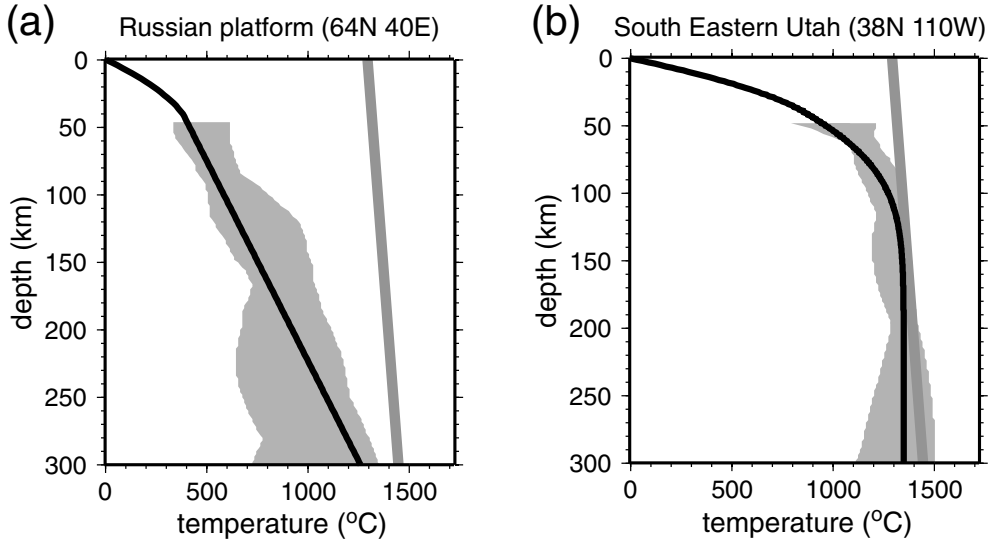

Figure 15. Temperature profiles inferred from the seismic model constrained by heat-flow data beneath (a) the Russian Platform (see Fig. 7b for the seismic model) and (b) southeastern Utah (see Fig. 9 for the seismic model). The shaded areas define the range of acceptable temperatures at each depth. In (a), the solid black line is the solution of the 1-D steady-state thermal equation (eq. B5) and in (b) it is the solution of the 1-D thermal equation (eq. B3) with a cooling age of 50 Myr. The thick gray lines are the 1300 °C adiabat, for reference.

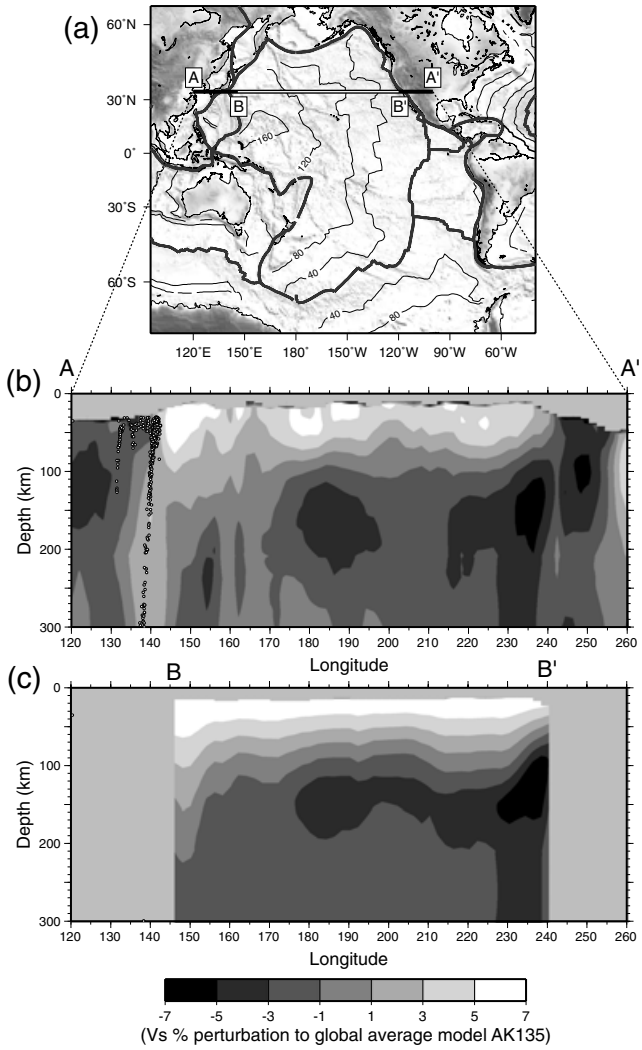

Figure 16. Vertical cross-section across the Pacific along the line indicated in (a), comparing the seismic model obtained with (b) the ad-hoc seismic parametrization of Shapiro & Ritzwoller (2002) and (c) the thermal parametrization in which the thermodynamic constraint on the temperature profile has been applied. Shear speeds are per cent perturbation relative to the 1-D model ak135.

Generic Mapping Tools (GMT) data processing and display package (Wessel & Smith 1991, 1995). Aspects of this work were supported by grants NSF-OPP-9615139 and NSF-OPP-9818498 from the Office of Polar Programs and NSF-EAR-0207753 from the Division of Earth Sciences at the US National Science Foundation, and Defense Threat Reduction Agency contracts DTRA01-99-C-0019 and DTRA01-00-C-0013.

REFERENCES

Artemieva, I.M. & Mooney, W.D., 2001. Thermal thickness and evolution of Precambrian lithosphere: A global study, *J. geophys. Res.,* **106,** 16 387–16,414.

Barmin, M.P., Ritzwoller, M.H. & Levshin, A.L., 2001. A fast an reliable method for surface wave tomography, *Pure appl. Geophys.,* **158,** 1351–1375.

Canas, J.A. & Mitchell, B.J., 1981. Rayleigh-wave attenuation and its variation across the Atlantic ocean, *Geophys. J. R. astr. Soc.,* **67,** 159–176.

Chan, W.W., Sacks, I.S. & Morrow, R., 1989. Anelasticity of the Iceland plateau from surface wave analysis, *J. geophys. Res.,* **94,** 5675–5688.

Dahlen, F.A. & Tromp, J., 1998. *Theoretical Global Seismology*, Princeton University Press, Princeton, NJ.

Deal, M.M. & Nolet, G., 1996. Nullspace shuttles, *Geophys. J. Int.,* **124,** 372–380.

Deal, M.M. & Nolet, G., 1999. Slab temperature and thickness from seismic tomography 2. Izu-Bonin, Japan, and Kuril subduction zones, *J. geophys. Res.,* **104,** 28 803–28 812.

Deal, M.M., Nolet, G. & van der Hilst, R.D., 1999. Slab temperature and thickness from seismic tomography 1. Method and application to Tonga, *J. geophys. Res.,* **104,** 28 789–28 802.

Dick, H.J.B., Fisher, R.L. & Bryan, W.B., 1984. Mineralogic variability of the uppermost mantle along mid-oceanic ridges, *Earth planet. Sci. Lett.,* **69,** 88–106.

Duffy, T.S. & Anderson, D.L., 1989. Seismic velocities in mantle minerals and the mineralogy of the upper mantle, *J. geophys. Res.,* **94,** 1895–1912.

Ekström, G. & Dziewonski, A.M., 1998. The unique anisotropy of the Pacific upper mantle, *Nature,* **394,** 168–172.

Ekström, G., Tromp, J. & Larson, E.W.F., 1997. Measurements and global models of surface waves propagation, *J. geophys. Res.,* **102,** 8137–8157.

Furlong, K.P., Spakman, W. & Wortel, R., 1995. Thermal structure of the continental lithosphere: constraints from seismic tomography, *Tectonophysics,* **244,** 107–117.

Goes, S., Govers, R. & Vacher, R., 2000. Shallow mantle temperatures under Europe from P and S wave tomography, *J. geophys. Res.,* **105,** 11 153–11 169.

Karato, S., 1993. Importance of anelasticity in the interpretation of seismic tomography, *Geophys. Res. Lett.,* **20,** 1623–1626.

Karato, S. & Jung, H., 1998. Water, partial melting and the origin of the seismic low velocity and high attenuation zone in the upper mantle, *Earth planet. Sci. Lett.,* **157,** 193–207.

Kennett, B.L.N., Engdahl, E.R. & Buland, R., 1995. Constraints on seismic velocities in the Earth from travel times, *Geophys. J. Int.,* **122,** 403–416.

McDonough, W.F. & Rudnick, R.L., 1998. Mineralogy and composition of the upper mantle, in *Ultrahigh-pressure mineralogy: physics and chemistry of the Earth's deep interior*, pp. 139–164, ed. Hemley, R.J., Mineralogical Society of America, Washington, DC.

Minister, J.B. & Anderson, D.L., 1981. A model of dislocation-controlled rheology for the mantle, *Phil. Trans. R. Soc. Lond.,* **299,** 319–356.

Mooney, W.D., Laske, G. & Masters, G., 1998. CRUST5.1: A global crustal model at 5° × 5°, *J. geophys. Res.,* **103,** 727–747.

Mueller, R.D., Roest, W.R., Royer, J.-Y., Gahagan, L.M. & Sclater, J.G., 1997. Digital isochrons of the world's ocean floor, *J. geophys. Res.,* **102,** 3211–3214.

Nyblade, A.A. & Pollack, H.N., 1993. A global analysis of heat flow from Precambrian terrains: implications for the thermal structure of Archean and Proterozoic lithosphere, *J. geophys. Res.,* **98,** 12 207–12 218.

Parsons, B. & Slater, J.G., 1977. An analysis of the variation of ocean floor bathymetry with age, *J. geophys. Res.,* **82,** 803–827.

Pollack, H.N., Hurter, S.J. & Johnson, J.R., 1993. Heat flow from the Earth's interior: analysis of the global data set, *Rev. Geophys.,* **31,** 267–280.

Ritzwoller, M.H. & Levshin, A.L., 1998. Eurasian surface wave tomography: Group velocities, *J. geophys. Res.,* **103,** 4839–4878.

Ritzwoller, M.H., Shapiro, N.M., Levshin, A.L. & Leahy, G.M., 2001. The structure of the crust and upper mantle beneath Antarctica and the surrounding oceans, *J. geophys. Res.,* **106**(B12), 30 645–30 670.

Ritzwoller, M.H., Shapiro, N.M., Barmin, M.P. & Levshin, A.L., 2002. Global surface wave diffraction tomography, *J. geophys. Res.,* **107**(B12), 2335, doi: 1029/2002JB001777.

Ritzwoller, M.H., Shapiro, N.M. & Leahy, G.M., 2003. A resolved mantle anomaly as the cause of the Australian-Antarctic Discordance, *J. geophys. Res.,* **108**(B12), 2559, 10.1029/2003JB002522.

Ritzwoller, M.H., Shapiro, N.M. & Zhong, S., 2004. Cooling history of the Pacific lithosphere, *J. geophys. Res.,* submitted.

Röhm, A.H.E., Snieder, R., Goes, S. & Trampert, J., 2000. Thermal structure of continental upper mantle inferred from *S*-wave velocity and surface heat flow, *Earth planet. Sci. Lett.,* **181,** 395–407.

Rudnick, R.L., McDonough, W.F. & O'Connell, R.J., 1998. Thermal structure, thickness and composition of continental lithosphere, *Chem. Geol.,* **145,** 395–411.

Shapiro, N.M. & Ritzwoller, M.H., 2002. Monte-Carlo inversion for a global shear velocity model of the crust and upper mantle., *Geophys. J. Int.,* **151,** 88–105.

Shapiro, N.M., Ritzwoller, M.H., Mareschal, J.-C. & Jaupart, C., 2004. Lithospheric structure of the Canadian Shield inferred from inversion of surface-wave dispersion with thermodynamic a priori constraints, *J. geol. Soc. Lond. Spec. Pub.*, accepted. Geological Prior Information, ed. R. Wood and A. Curtis.

Sobolev, S.V., Zeyen, H., Stoll, G., Werling, F., Altherr, R. & Fuchs, K., 1996. Upper mantle temperatures from teleseismic tomography of French Massif Central including effects of composition, mineral reactions, anharmonicity, anelasticity and partial melt., *Earth planet. Sci. Lett.,* **157,** 193–207.

Spencer, C. & Gubbins, D., 1980. Travel-time inversion for simultaneous earthquake location and velocity structure determination in laterally varying media, *Geophys. J. R. astr. Soc.,* **63,** 95–116.

Stein, C.A. & Stein, S., 1992. A model for the global variation in oceanic depth and heat flow with lithospheric age, *Nature,* **359,** 123–129.

Trampert, J. & Woodhouse, J.H., 1995. Global phase velocity maps of Love and Rayleigh waves between 40 and 150 s period, *Geophys. J. Int.,* **122,** 675–690.

Trampert, J., Vacher, P., and Vlaar, N., 2001. Sensitivities of seismic velocities to temperature, pressure, and composition of the lower mantle, *Phys. Earth planet. Int.,* **124,** 255–267.

Turcotte, D.L. & G., Schubert, 1982. *Geodynamics. Applications of continuum physics to geological problems*, John Wiley & Sons, New York.

van Wijk, J.W., Govers, R. & K.P. Furlong, 2001. Three-dimensional thermal modeling of the California upper mantle: a slab window vs. stalled slab, *Earth planet. Sci. Lett.,* **186,** 175–186.

Wessel, P. & Smith, W.H.F., 1991. Free software helps map and display data, *EOS, Trans. Am. geophys. Un.,* **72,** 441.

Wessel, P. & Smith, W.H.F., 1995. New version of the Generic Mapping Tools released, *EOS, Trans. Am. geophys. Un.,* **76,** 329.

Yan, B., Graham, E.K. & Furlong, K.P., 1989. Lateral variations in upper mantle thermal structure inferred from three-dimensional seismic inversion models, *Geophys. Res. Lett.,* **16,** 449–452.

APPENDIX A: CONVERSION BETWEEN SEISMIC VELOCITIES AND TEMPERATURE

A1 Anharmonicity

We consider the mantle to be composed of five principal minerals: olivine, orthopyroxene, clinopyroxene, garnet and spinel. For each mineral, we calculate the elastic moduli μ and K and density ρ as functions of temperature T, pressure P and iron content X based on the following equations:

$$\mu(P,T,X) = \mu_0 + (T-T_0)\frac{\partial\mu}{\partial T} + (P-P_0)\frac{\partial\mu}{\partial P} + X\frac{\partial\mu}{\partial X}, \quad \text{(A1)}$$

$$K(P,T,X) = K_0 + (T-T_0)\frac{\partial K}{\partial T} + (P-P_0)\frac{\partial K}{\partial P} + X\frac{\partial K}{\partial X}, \quad \text{(A2)}$$

$$\rho(P,T,X) = \rho_0(X)\left[1 - \alpha(T-T_0) + \frac{(P-P_0)}{K}\right], \quad \text{(A3)}$$

$$\rho_0(X) = \rho_0|_{X=0}\frac{\partial\rho}{\partial X}, \quad \text{(A4)}$$

$$\alpha(T) = \alpha_0 + \alpha_1 T + \alpha_2 T^{-1} + \alpha_3 T^{-2}. \quad \text{(A5)}$$

The coefficient of thermal expansion is denoted by α and the subscript 0 refers to the values of a quantity at the P–T condition at the Earth's surface with zero iron content. The following quantities and their partial derivatives are defined from laboratory experiments (see Goes *et al.* 2000, for a summary):

$$\rho_0|_{X=0},\ \mu_0,\ K_0,\ \frac{\partial\rho}{\partial X},\ \frac{\partial\mu}{\partial X},\ \frac{\partial K}{\partial X},\ \frac{\partial\rho}{\partial T},\ \frac{\partial\mu}{\partial T},\ \frac{\partial K}{\partial T},\ \frac{\partial\rho}{\partial P},\ \frac{\partial\mu}{\partial P},\ \frac{\partial K}{\partial P},\ \alpha_0,\alpha_1,\alpha_2,\alpha_3. \quad \text{(A6)}$$

The average elastic moduli and density for a given mantle composition are calculated based on volumetric proportions of individual minerals λ_i and the Voigt–Reuss–Hill averaging scheme:

$$\langle\rho\rangle = \sum\lambda_i\rho_i, \quad \text{(A7)}$$

$$\langle\mu\rangle = \frac{1}{2}\left[\sum\lambda_i\mu_i + \left(\frac{\lambda_i}{\mu_i}\right)^{-1}\right], \quad \text{(A8)}$$

$$\langle K\rangle = \frac{1}{2}\left[\sum\lambda_i K_i + \left(\frac{\lambda_i}{K_i}\right)^{-1}\right]. \quad \text{(A9)}$$

With the following standard relations

$$v_p = \sqrt{K + \frac{4}{3}\mu/\rho} \qquad v_s = \sqrt{\mu/\rho}, \quad \text{(A10)}$$

we obtain seismic velocities as functions of iron content, mineralogical composition, temperature and pressure, which is equivalent to depth if we neglect lateral pressure variations.

A2 Anelasticity

Anharmonic effects represent only one part of the velocity–temperature relation. At high mantle temperatures, anelasticity contributes significantly (e.g. Karato 1993). The anelastic behaviour of mantle materials results in the attenuation of seismic waves and also affects the seismic velocities. Its effect is generally described in terms of the quality factor Q. We use the mantle attenuation model of Minister & Anderson (1981) in which shear quality factor within an absorption band is written as a function of temperature and pressure:

$$Q_\mu(P,T,\omega) = A\omega^a \exp[a(H^* + PV^*)/RT], \quad \text{(A11)}$$

where A and a are constants, H^* is the activation energy, V^* is the activation volume and ω is frequency. During the surface wave inversion, the velocity model is produced at unit frequency, therefore $\omega = 2\pi$. The P-wave quality factor is

$$Q_P = \frac{3}{4}\frac{v_s^2}{v_p^2}Q_\mu. \quad \text{(A12)}$$

The velocity correction associated with anelastic attenuation is performed in the following way:

$$v_{\text{anel}}(P,T,\omega) = v(P,T,\omega)\left[1 - \frac{2Q^{-1}(P,T,\omega)}{\tan(\pi a/2)}\right], \quad \text{(A13)}$$

where v is v_p or v_s and Q is Q_μ or Q_P, respectively. As shown in Fig. A1, this correction becomes less than 1 per cent for

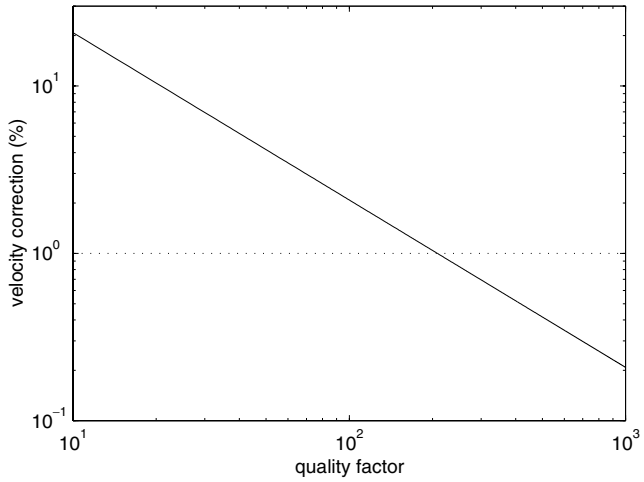

Figure A1. Anelastic velocity correction as predicted by eq. (A13).

$Q > 200$. Following Sobolev *et al.* (1996), we use $= 0.15$, $H^* = 500$ kJ mol^{-1}, and $V^* = 2.0 \times 10^{-5}$ m^3 mol^{-1}. However, we re-calibrated the constant A. Sobolev *et al.* (1996) calibrated their attenuation model to fit certain measurements of the seismic quality factor and found $A = 0.148$. We prefer to calibrate the anelastic correction based on seismic velocity measurements and use our global model (Shapiro & Ritzwoller 2002), which has an average shear velocity of 4.4 km s^{-1} at 200 km depth. With an average mantle temperature at this depth of 1400 °C, to fit this shear velocity we obtain $A \approx 0.049$. This value of A tends to reduce Q and strengthens the anelastic correction.

APPENDIX B: THERMAL MODEL OF THE CRUST AND THE UPPER MANTLE

Below the Earth's surface, the temperature increases rapidly with depth. As a consequence, the viscosity decreases very rapidly with depth in the shallow part of the upper mantle. This strong viscosity gradient results in different regimes of heat transfer. In the high-viscosity lithosphere, heat transfer is dominated by conduction while convective heat transfer is more effective in the deeper part of the mantle with lower viscosity.

B1 CONVECTIVE MANTLE

If convection occurs adiabatically, the temperature in the convective part of the upper mantle increases approximately linearly with depth z (Fig. A2):

$$T = T_p + D_a z, \tag{B1}$$

where T_p is the potential temperature and D_a is the adiabatic gradient that can be expressed as (e.g. Turcotte & Schubert 1982):

$$D_a = \frac{\alpha g T_a}{c_p}, \tag{B2}$$

where α is the coefficient of thermal expansion, T_a is the average temperature of the convective upper mantle, g is the acceleration of gravity and c_p is the specific heat.

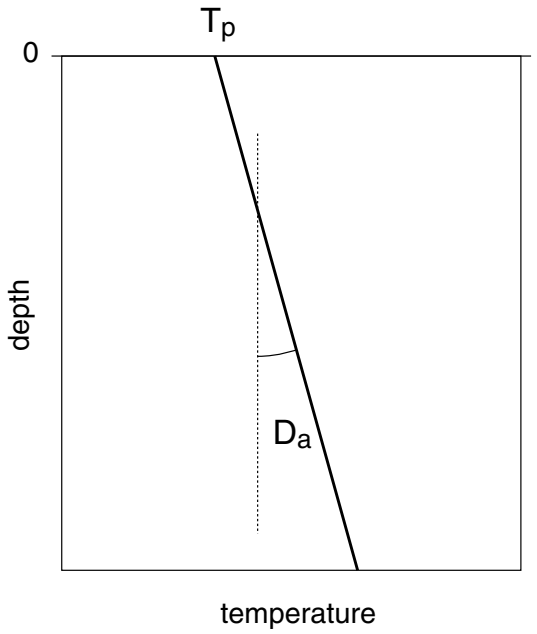

Figure A2. Schematic geotherm in the convective mantle, see eq. (B1), where T_p is potential temperature, D_a is the adiabatic gradient, and depth and temperature range over values appropriate to the convective part of the model (see Fig. 10).

B2 Conductive lithosphere

If we neglect lateral temperature variations, the temperature within the lithosphere is controlled by the 1-D thermal conductivity equation:

$$\frac{\partial T}{\partial t} = \kappa \frac{\partial^2 T}{\partial z^2} + \frac{\kappa}{k} H, \tag{B3}$$

with the boundary condition

$$T|_{z=0} = 0, \tag{B4}$$

where κ is the thermal diffusivity (set to 1.0×10^{-6} m^2 s^{-1}), T is temperature, t is time, z is depth, H is the volumetric heat production and k is thermal conductivity.

We consider two types of solutions to this thermal equation. The first is the steady-state solution when the temporal derivative in eq. (B3) equals zero and the conductivity equation becomes:

$$\frac{\partial^2 T(z)}{\partial z^2} = -H(z)/k. \tag{B5}$$

In a stationary regime, surface heat flow, q_0, results in an additional boundary condition:

$$q_0 = k \left. \frac{\partial T}{\partial z} \right|_{z=0}. \tag{B6}$$

The solution of eq. (B5) with boundary conditions eqs (B4) and (B6) depends on three parameters: the surface heat flow q_0, the radioactive heat production H and the thermal conductivity k. As shown in Fig. A3, higher heat flow implies higher mantle temperatures, while higher heat production and thermal conductivity results in lower temperatures if heat flow is held constant.

We also consider a time-dependent cooling solution of eq. (B3). In this case, the initial condition is a constant temperature T_m. The cooling solution depends on this initial mantle temperature T_m, the

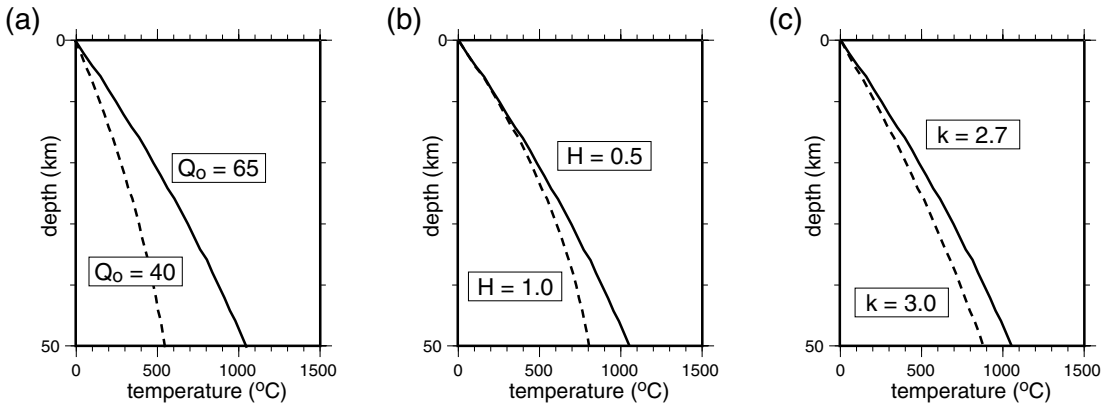

Figure A3. Solutions of the 1-D thermal steady-state eq. (B5) with boundary conditions eqs (B4) and (B6). (a) Effect of surface heat flow. Solid and dashed lines show solutions obtained with $Q_0 = 65$ mW m^{-2} and $Q_0 = 40$ mW m^{-2}, respectively. In both cases, $H = 0.5$ μW m^{-3} and $k = 2.7$ W m^{-1} K^{-1}. (b) Effect of internal heat production. Solid and dashed lines show solutions obtained with $= 0.5$ μW m^{-3} and $H = 1.0$ μW m^{-3}, respectively. In both cases, $Q_0 = 65$ mW m^{-2} and $k = 2.7$ W m^{-1} K^{-1}. (c) Effect of thermal conductivity. Solid and dashed lines show solutions obtained with $k = 2.7$ W m^{-1} K^{-1} and $k = 3.0$ W m^{-1} K^{-1}, respectively. In both cases, $Q_0 = 65$ mW m^{-2} and $H = 0.5$ μW m^{-3}.

time of cooling called here the cooling age τ_c and the thermal conductivity, the thermal diffusivity and the heat production in the crust and upper mantle. In the general case, the solution of the eq. (B3) can be easily found numerically. However, in the simplest case of a homogeneous half-space without internal heat production the cooling solution takes a simple analytical form known as the half-space cooling model (e.g. Turcotte & Schubert 1982):

$$T(z) = T_s + (T_m - T_s)\mathrm{erf}\left(\frac{z}{2\sqrt{\kappa \tau_c}}\right), \tag{B7}$$

where T_s is the surface temperature. This model can be reasonably applied to the oceanic lithosphere where the radioactive heat production is very low and the crust is very thin. If we fix the mantle thermal diffusivity, the half-space cooling solution depends on two parameters: τ_c and T_m. However, these two parameters are not completely independent. Fig. A4 shows two half-space cooling temperature profiles, one with a cooling age $\tau_c = 90$ Myr and mantle temperature $T_m = 1300$ °C and the other with $\tau_c = 110$ Myr and $T_m = 1400$°C. These profiles are nearly indistinguishable at low temperatures (<1100 °C) where the the heat transfer is expected to be conductive. This low-temperature part of the profile can be represented with a variety of combinations of τ_c and T_m because larger thermal ages can be compensated by higher mantle temperatures.

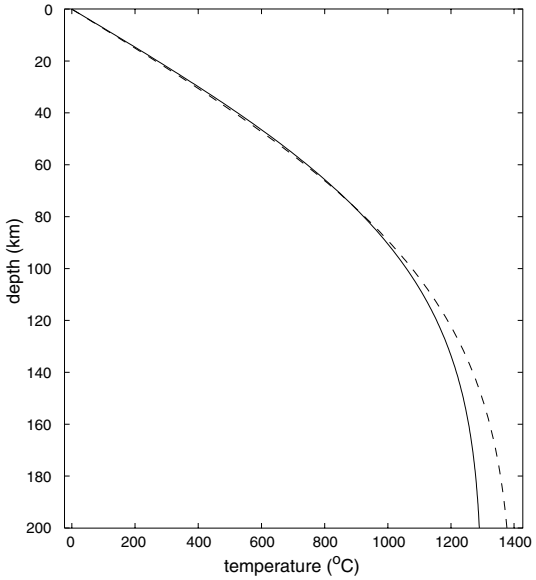

Figure A4. Half-space cooling models (eq. B7) with different cooling ages τ_c and mantle temperatures T_M. Solid line corresponds to $T_m = 1300$ °C and $\tau_c = 90$ Myr, and dashed line corresponds to $T_m = 1400$ °C and $\tau_c = 110$ Myr.